6-24-2010

Morphotropic phase boundary and electrical properties of lead-free (1–x)BaTiO3–xBi(Li1/3Ti2/3)O3 ceramics

C. Ma
Iowa State University

Xiaoli Tan
Iowa State University, xtan@iastate.edu

Morphotropic phase boundary and electrical properties of lead-free (1−x)BaTiO3−xBi(Li1/3Ti2/3)O3 ceramics

Abstract
Dense polycrystalline ceramics of lead-free perovskitesolid solution(1−x)BaTiO3−xBi(Li1/3Ti2/3)O3 (0.05≤x≤0.20) have been synthesized via the conventional solid state reaction method. A morphotropic phase boundary separating the tetragonal and orthorhombic phases was observed between the compositions x=0.07 and 0.10. With increasing Bi(Li1/3Ti2/3)O3 content, the solid solution displays a stronger frequency dispersion in its dielectric behavior and a significant suppression in the sharp dielectric anomaly at the Curie point as well as the remanent polarization. However, the Curie point of the solid solution is almost independent of x in the composition range studied. These behaviors can be explained by the observed core-shell grain structure. The incorporation of Bi(Li1/3Ti2/3)O3 into BaTiO3 leads to the formation of nanodomains in the shell, which imparts the relaxor characteristics to the dielectric behavior. The core of the grain preserves the large lamellar domains as those in BaTiO3, contributing to the sharp transition at ~130 °C. The best piezoelectric coefficient was obtained in the composition x=0.07 with d33=110 pC/N.

Keywords
Ozone, Relaxor ferroelectrics, Solid solutions, Ceramics, Dielectric oxides, Dielectrics, Piezoelectricity, Polarization, Ferroelectric phase transitions, Ferroelectricity

Disciplines
Ceramic Materials | Materials Science and Engineering

Comments
The following article appeared in *Journal of Applied Physics* 107 (2010): 124108 and may be found at http://dx.doi.org/10.1063/1.3437215.

Morphotropic phase boundary and electrical properties of lead-free (1 x) BaTiO 3 x Bi (Li 1 / 3 Ti 2 / 3) O 3 ceramics

C. Ma and X. Tan

Citation: Journal of Applied Physics **107**, 124108 (2010); doi: 10.1063/1.3437215
View online: http://dx.doi.org/10.1063/1.3437215
View Table of Contents: http://scitation.aip.org/content/aip/journal/jap/107/12?ver=pdfcov
Published by the AIP Publishing

Morphotropic phase boundary and electrical properties of lead-free $(1-x)BaTiO_3-xBi(Li_{1/3}Ti_{2/3})O_3$ ceramics

C. Ma and X. Tan[a)]
Department of Materials Science and Engineering, Iowa State University, Ames, Iowa 50011, USA

(Received 19 December 2009; accepted 2 May 2010; published online 24 June 2010)

Dense polycrystalline ceramics of lead-free perovskite solid solution $(1-x)BaTiO_3-xBi(Li_{1/3}Ti_{2/3})O_3$ $(0.05 \leq x \leq 0.20)$ have been synthesized via the conventional solid state reaction method. A morphotropic phase boundary separating the tetragonal and orthorhombic phases was observed between the compositions $x=0.07$ and 0.10. With increasing $Bi(Li_{1/3}Ti_{2/3})O_3$ content, the solid solution displays a stronger frequency dispersion in its dielectric behavior and a significant suppression in the sharp dielectric anomaly at the Curie point as well as the remanent polarization. However, the Curie point of the solid solution is almost independent of x in the composition range studied. These behaviors can be explained by the observed core-shell grain structure. The incorporation of $Bi(Li_{1/3}Ti_{2/3})O_3$ into $BaTiO_3$ leads to the formation of nanodomains in the shell, which imparts the relaxor characteristics to the dielectric behavior. The core of the grain preserves the large lamellar domains as those in $BaTiO_3$, contributing to the sharp transition at ~130 °C. The best piezoelectric coefficient was obtained in the composition $x=0.07$ with $d_{33}=110$ pC/N. © *2010 American Institute of Physics*. [doi:10.1063/1.3437215]

I. INTRODUCTION

Lead-based piezoelectric ceramics, represented by $Pb(Zr,Ti)O_3$ (PZT), have been widely used in industry due to their excellent performances in piezoelectric, ferroelectric, and dielectric applications.[1–3] However, the significant amount of lead in these functional ceramics has raised environmental concerns, which has stimulated the world-wide intensive efforts in searching for lead-free piezoelectric ceramics.[4]

The success of PZT perovskite oxides for piezoelectric applications has demonstrated the importance of morphotropic phase boundary (MPB) and strong ferroelectricity in achieving high piezoelectric properties.[4–7] The presence of MPB offers a bridging monoclinic phase and disrupts the large ferroelectric domains,[5,8] both of which facilitate the polarization switching process. The strong ferroelectricity in PZT originates from A- and B-site cation off-center displacements. It was shown that the $6s^2$ lone pair of electrons of the A-site cation Pb^{2+} hybridize with an empty $2p$ orbital of O^{2-}, forming a localized lobe that causes off-center structural distortion and enhances ferroelectricity.[6,9] The empty d orbitals of B-site cations Zr^{4+} and Ti^{4+} can trigger the second-order Jahn–Teller distortion, which introduces ferroelectric distortion by off-center displacement of the cation.[7,9,10] Therefore, Bi^{3+} would be best to substitute Pb^{2+} in the A-site for lead-free perovskite piezoceramics because it also possesses the $6s^2$ lone pair of electrons, while B-site should be occupied by the cations with a d^0 electron configuration.[7,10,11] Bi-based perovskite compounds with d^0 B-site cations such as $BiScO_3$ and $Bi(Zn_{1/2}Ti_{1/2})O_3$ indeed have been reported to display strong ferroelectricity.[12–15]

Among the common d^0 B-site cations of Sc^{3+}, Ti^{4+}, Zr^{4+}, Nb^{5+}, and W^{6+}, Ti^{4+} is identified as the most active for ferroelectricity.[7] To include Bi^{3+} in the A-site and Ti^{4+} on the B-site in a perovskite structure for strong ferroelectricity, an additional B-site cation whose valence is lower than 3+ is needed to maintain the charge balance, as in the case of $Bi(Zn_{1/2}Ti_{1/2})O_3$ where 50% B-site is occupied by Ti^{4+}. An occupancy of Ti^{4+} on the B-site at a fraction higher than 50% has to be accompanied with a 1+ valence cation. Considering the appropriate size and the high tendency of off-center displacement in oxygen polyhedral cages of Li^+,[16,17] it appears that $Bi(Li_{1/3}Ti_{2/3})O_3$ might be a perovskite compound potentially displaying strong ferroelectricity. However, there have been no reports in literature on $Bi(Li_{1/3}Ti_{2/3})O_3$ or $Bi(Li_{1/3}Ti_{2/3})O_3$-based solid solutions. Similar to $BiScO_3$ and $Bi(Zn_{1/2}Ti_{1/2})O_3$,[12,18] $Bi(Li_{1/3}Ti_{2/3})O_3$ cannot be prepared as a perovskite ceramic at high temperatures under ambient pressures. In the present work, $BaTiO_3$ was employed to stabilize $Bi(Li_{1/3}Ti_{2/3})O_3$ in the perovskite structure. Within the solubility limit $(x=0.2)$ in the solid solution $(1-x)BaTiO_3-xBi(Li_{1/3}Ti_{2/3})O_3$, an MPB between tetragonal and orthorhombic perovskite phases was found and properties pertinent to piezoelectric applications were examined.

II. EXPERIMENTAL PROCEDURE

Polycrystalline ceramic samples of the solid solution $(1-x)BaTiO_3-xBi(Li_{1/3}Ti_{2/3})O_3$ $(0.05 \leq x \leq 0.20)$ were synthesized via the conventional solid state reaction method. The reagent grade powders of Bi_2O_3 (≥99.9%,Sigma-Aldrich), Li_2CO_3 (≥99.4%, Fisher Scientific), TiO_2 (≥99.99%,Sigma-Aldrich) and $BaCO_3$ (≥99.99%,Alfa Aesar) were used as starting materials. Stoichiometric amount of powders were mixed and vibratory milled in ethanol with zirconia mill media for 7 h and then dried. The Li_2CO_3 powder was baked at 200 °C for 15 h and then weighed immediately. The mixture was calcined at 900 °C for 5 h and then vibratory milled for another 16 h. After drying, the powders were evenly mixed with the binder (10 wt % polyvinyl alco-

[a)]Author to whom correspondence should be addressed. Electronic mail: xtan@iastate.edu.

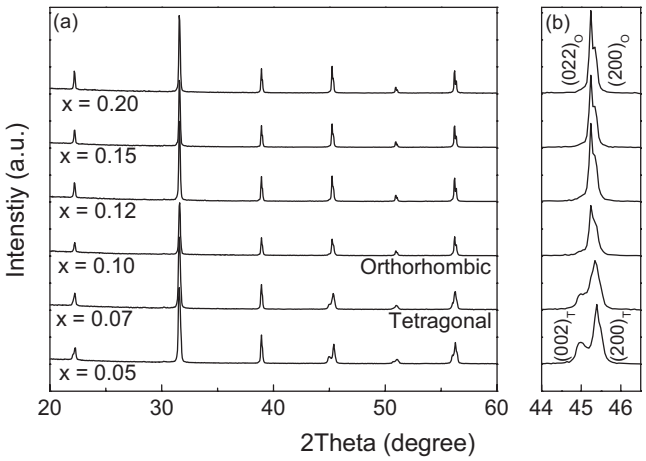

FIG. 1. XRD patterns of $(1-x)BaTiO_3-xBi(Li_{1/3}Ti_{2/3})O_3$ sintered samples in the range of 2θ (a) from 20° to 60° and (b) from 44.0° to 46.5°.

hol solution) and then uniaxially pressed into pellets at 300 MPa. Following the binder burnout at 500 °C, the sintering was carried out at 1150 °C for 4 h to obtain dense ceramic pellets. In order to minimize the loss of Bi^{3+} and Li^+, the pellets were buried in the protective powder with the same composition during sintering.

Surface layers of thickness ~400 μm were removed from the as-sintered pellets by mechanical grinding before the x-ray diffraction (XRD) analysis, which was performed on a PANalytical X'pert PRO MPD x-ray diffractometer with monochromatic Cu $K\alpha$ radiation in the step scanning mode with increments of 0.05°. Prior to the electrical measurements, both sides of the sample were polished and made parallel. Silver paste (Dupont 6160) was then fired on both sides at 850 °C for 5 min. Dielectric characterization was performed with an LCR meter (HP-4284A, Hewlett-Packard) in conjugation with a tube furnace. A heating rate of 3 °C/min was used during the measurement. The polarization hysteresis loop measurement was performed at room temperature with a frequency of 4 Hz using a standardized ferroelectric test system (RT-66A, Radiant Technologies). Before the piezoelectric measurement, samples were poled by a field cooling process under 30 kV/cm from 140 °C to room temperature. The piezoelectric coefficient d_{33} was measured with a piezo-d_{33} meter (ZJ-4B, Shanghai Institute of Ceramics, China) 24 h after poling.

Transmission electron microscopy (TEM) specimens were prepared from the ultrasonically cut disks with diameter of 3 mm. The central portion of the disk was mechanically polished and dimpled to 5 μm thick. The dimpled disk was then annealed at 250 °C for 2 h to minimize the residual stresses introduced during mechanical thinning. Finally the disk was Ar-ion milled to electron transparency. The TEM study was carried out on a Phillips CM-30 microscope operated at 300 kV with a Gatan charge coupled device camera installed.

III. RESULTS AND DISCUSSION

Figure 1(a) displays the XRD pattern of the sintered ceramics of different compositions. All of the samples are phase-pure with a perovskite structure. No additional diffraction peaks which could suggest the presence of superstructure or impurity phases were observed from the XRD patterns. This indicates that $Bi(Li_{1/3}Ti_{2/3})O_3$ has completely diffused into the lattice of $BaTiO_3$ and formed a solid solution. Attempts of synthesizing phase-pure $(1-x)BaTiO_3-xBi(Li_{1/3}Ti_{2/3})O_3$ ceramics with $x>0.20$ using conventional sintering failed, suggesting a solubility limit of $x=0.20$. Close examination of the Bragg peak 2θ at around 45° [Fig. 1(b)] reveals that the ceramics with $x\leq 0.07$ display a tetragonal distortion as characterized by its $(002)_T/(200)_T$ peak splitting, while those with $x\geq 0.10$ are stabilized in an orthorhombic symmetry as characterized by the $(022)_O/(200)_O$ peak splitting. An MPB is thus located between the composition $x=0.07$ and 0.10.

The temperature dependence of the dielectric constant ε_r and loss $\tan\delta$ at a series of frequencies is displayed in Fig. 2. For all the compositions, the position of the anomaly in the ε_r versus T curves remains almost unchanged at ~130 °C, which marks the ferroelectric-paraelectric transition at the Curie point T_C. However, its contribution to the dielectric constant gets weaker as the $Bi(Li_{1/3}Ti_{2/3})O_3$ content increases. At the same time, a relaxor ferroelectric behavior with a diffused transition at a lower temperature T_m gets stronger in the solid solution $(1-x)BaTiO_3-xBi(Li_{1/3}Ti_{2/3})O_3$: nontrivial frequency dispersion in the dielectric behavior was observed for $x\geq 0.07$ and increases with increasing x. A strong frequency dependence of T_m is observed from Fig. 2. In the composition $x=0.20$, the diffused relaxor transition at T_m overwhelms the ferroelectric-paraelectric transition at 130 °C to dominate the dielectric behavior.

The introduction of relaxor behaviors to $BaTiO_3$ by incorporation of $Bi(Li_{1/3}Ti_{2/3})O_3$ can be quantified by fitting the dielectric constant ε_r with the following expression:[19,20]

$$\frac{\varepsilon_m}{\varepsilon_r}-1=\frac{(T-T_m)^\gamma}{2\delta^2}, \tag{1}$$

where γ is the degree of dielectric relaxation, which equals to 1 for a normal ferroelectric and 2 for an ideal ferroelectric relaxor, δ is the degree of diffuseness of the transition, ε_m is the maximum value of the dielectric constant, and T_m is the temperature where the dielectric constant reaches ε_m. Since T_m is well below T_C in $(1-x)BaTiO_3-xBi(Li_{1/3}Ti_{2/3})O_3$, T_m in Eq. (1) is replaced with T_C and ε_m in Eq. (1) is taken as the dielectric constant at T_C. Figure 3(a) displays the $(\varepsilon_m/\varepsilon_r-1)$ versus $(T-T_C)$ plots in log scale using the ε_r versus T data at 1 MHz in the range from 140 to 330 °C. The linear relationship was observed in the curves of all the compositions. The parameters γ and δ determined from linear fitting are displayed in Fig. 3(b). Obviously the increase in the content of $Bi(Li_{1/3}Ti_{2/3})O_3$ in the solid solution leads to a monotonic increase in the degree of the diffuseness of the transition. Although with fluctuations, the relaxation parameter γ also follows this general trend. This observation supports the conclusion that the $(1-x)BaTiO_3-xBi(Li_{1/3}Ti_{2/3})O_3$ solid solution becomes more of a ferroelectric relaxor as x increases. The relaxor behavior might be attributed to the presence of Bi^{3+} on the A-site and Li^+ on the

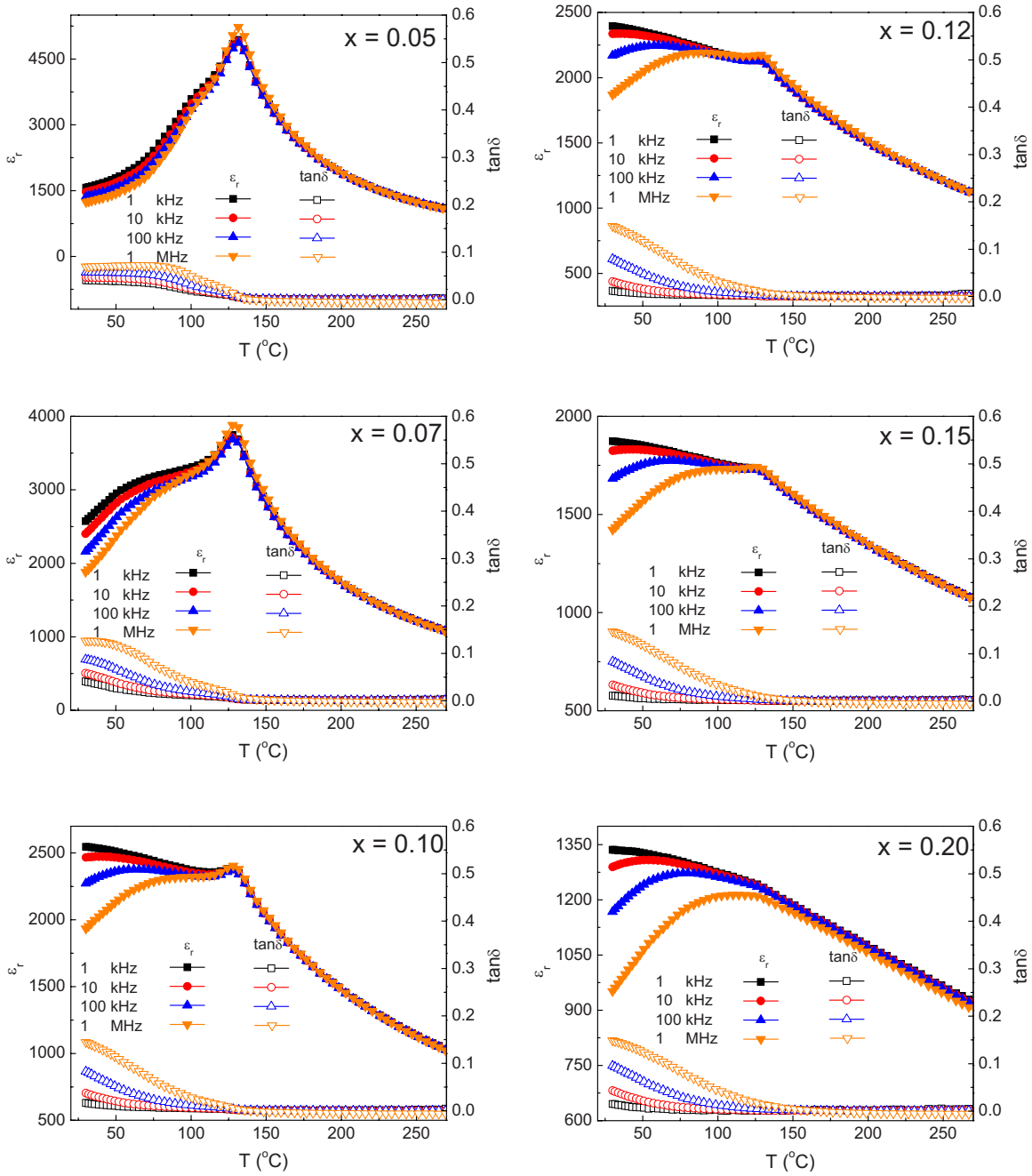

FIG. 2. (Color online) Temperature dependence of dielectric constant ε_r and loss $\tan\delta$ of $(1-x)BaTiO_3-xBi(Li_{1/3}Ti_{2/3})O_3$ ceramics measured at 1 kHz, 10 kHz, 100 kHz, and 1 MHz.

B-site, both of which are aliovalent cations with random occupancy.

In order to find the microstructural origin for the two successive transitions at T_m and T_C, a TEM study was performed on the composition $x=0.10$, which exhibits comparable dielectric permittivity at the diffused transition at T_m and the sharp transition at T_C. The TEM results of a representative grain tilted to its [011], [111], and $[\bar{1}11]$ zone axes are shown in Fig. 4. A core-shell grain structure with large lamellar domains in the core and nanodomains in the shell was observed. This core-shell structure was found to be a general feature for all grains imaged in this specimen. The core of the grain in Fig. 4 exhibits two sets of ferroelectric domains. When tilted to its [111] zone axis, the set of domains in the left have their walls at edge-on position. When tilted to its $[\bar{1}11]$ zone axis, the set in the right is edge-on. The crystallographic planes of these two sets of domain walls are thus determined to be $(1\bar{1}0)$ and (110), respectively. Therefore, these are 90° ferroelectric domains. The electron diffraction patterns from the core and shell appear identical, with no superlattice spots present in all zone axes.

Generally speaking, large lamellar ferroelectric domains correspond to a normal ferroelectric behavior with a sharp transition and nanodomains often lead to the relaxor behavior with a diffused transition.[21,22] The incorporation of $Bi(Li_{1/3}Ti_{2/3})O_3$ into $BaTiO_3$ forms nanodomains in the volume close to grain boundaries because the solid state reac-

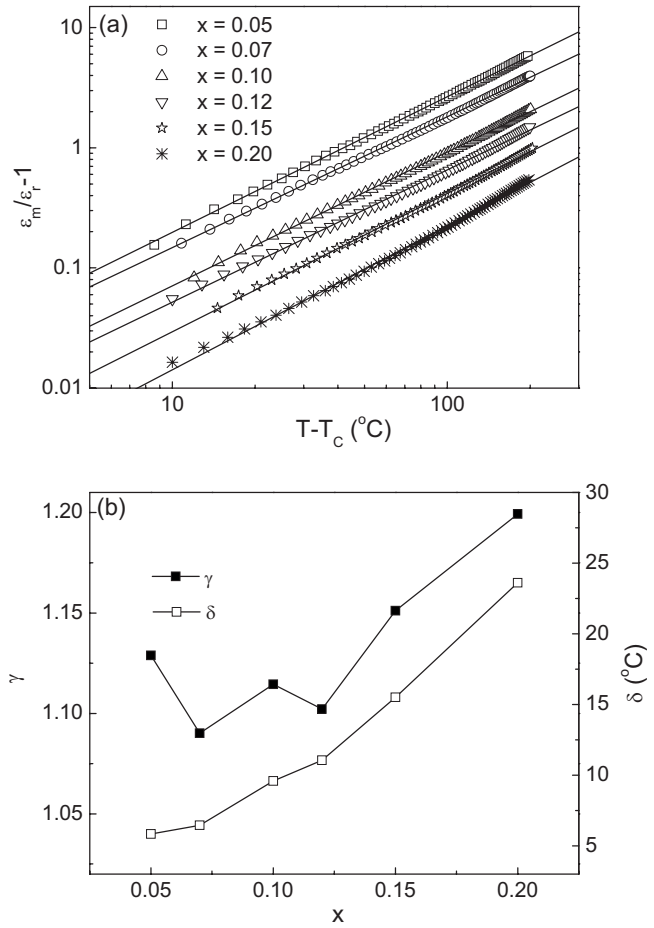

FIG. 3. (a) Plot of $(\varepsilon_m/\varepsilon_r-1)$ vs $(T-T_C)$ in log scale using the ε_r vs T data obtained at 1 MHz in the temperature range of 140–330 °C in $(1-x)BaTiO_3-xBi(Li_{1/3}Ti_{2/3})O_3$ ceramics. The symbols represent the experimental data, while the solid lines are the linear fit. (b) The relaxation parameter γ and the diffuseness parameter δ determined by the data fitting.

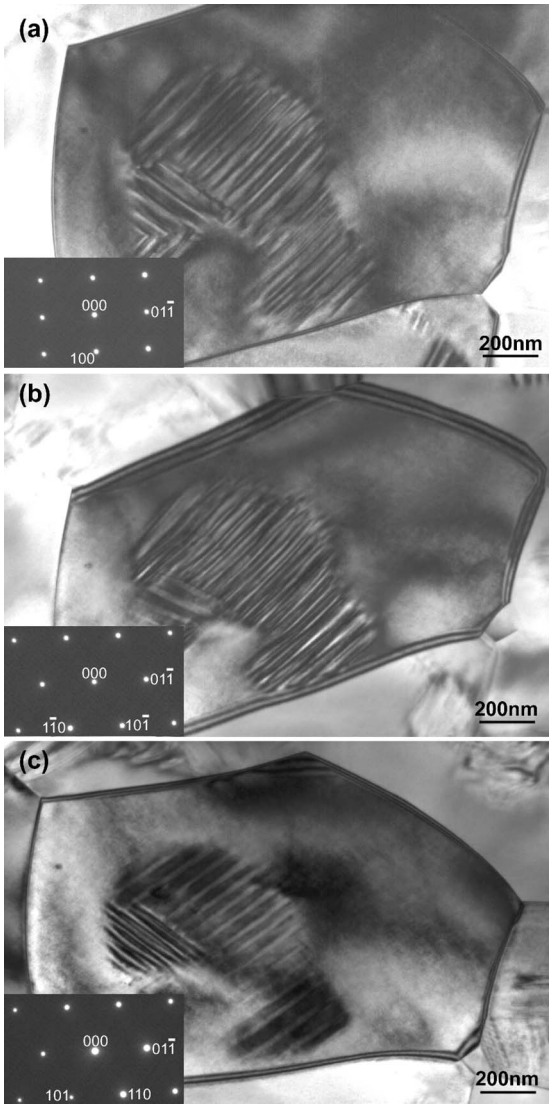

FIG. 4. TEM bright field images of a representative grain for $x=0.10$ tilted to its (a) [011], (b) [111], and (c) $[\bar{1}11]$ zone axes. The insets are the corresponding electron diffraction patterns.

tion starts from particle surfaces during calcination and diffusion is faster along grain boundaries during sintering. The diffusion process is not complete at the end of sintering and the core of the grain is largely pure $BaTiO_3$ with minimum amount of $Bi(Li_{1/3}Ti_{2/3})O_3$. As a result, the temperature for the dielectric anomaly caused by the ferroelectric-paraelectric transition of the core stays at ~130 °C. As the content of $Bi(Li_{1/3}Ti_{2/3})O_3$ increases, the volume fraction of the core with regular lamellar ferroelectric domains becomes smaller and eventually diminishes at $x=0.20$. Therefore, the relaxor behavior contributed by the shell with nanodomains becomes more and more dominant in the ε_r versus T curve. Because of the heterogeneous microstructure and composition variation within individual grains in $(1-x)BaTiO_3-xBi(Li_{1/3}Ti_{2/3})O_3$, ferroelectric phase transitions occur at two distinct temperatures T_m and T_C. Similar behaviors have been previously observed in $(1-x)BaTiO_3-xBiScO_3$.[13]

The change from a normal ferroelectric to a relaxor behavior in $(1-x)BaTiO_3-xBiScO_3$ (Ref. 13) and $(1-x)BaTiO_3-xBi(Zn_{1/2}Ti_{1/2})O_3$ (Ref. 15) was found to correspond to a change from tetragonal to pseudocubic crystal structure at room temperature. However, the enhanced relaxor behavior in $(1-x)BaTiO_3-xBi(Li_{1/3}Ti_{2/3})O_3$ is accompanied with an orthorhombic crystal structure at room temperature, as shown in Fig. 1. This resembles the situation in the $(1-x)BaTiO_3-xBaZrO_3$ solid solution where the orthorhombic phase is stabilized at room temperature in $Ba(Ti_{0.95}Zr_{0.05})O_3$.[23] Thus the incorporation of $Bi(Li_{1/3}Ti_{2/3})O_3$ into $BaTiO_3$ shifts the tetragonal-orthorhombic phase transition of $BaTiO_3$ to higher temperatures. The transition occurs at a temperature below room temperature in compositions $x=0.05$ and 0.07 and above room temperature in compositions $x\geq 0.10$. Maybe it is associated with the emergence of the relaxor behavior, this tetragonal-orthorhombic phase transition is found hard to be connected to a specific anomaly in the ε_r versus T curves.

Figure 5 displays the electrical polarization P versus electric field E hysteresis loops for samples of different compositions measured at room temperature. The remanent polarization P_r reaches 10.8 $\mu C/cm^2$ for the sample with $x=0.05$, which is larger than the previously reported P_r (~7 $\mu C/cm^2$) for pure $BaTiO_3$.[1] However, further increase in the $Bi(Li_{1/3}Ti_{2/3})O_3$ content leads to a sharp decrease in both remanent polarization P_r and the coercive field E_C. The

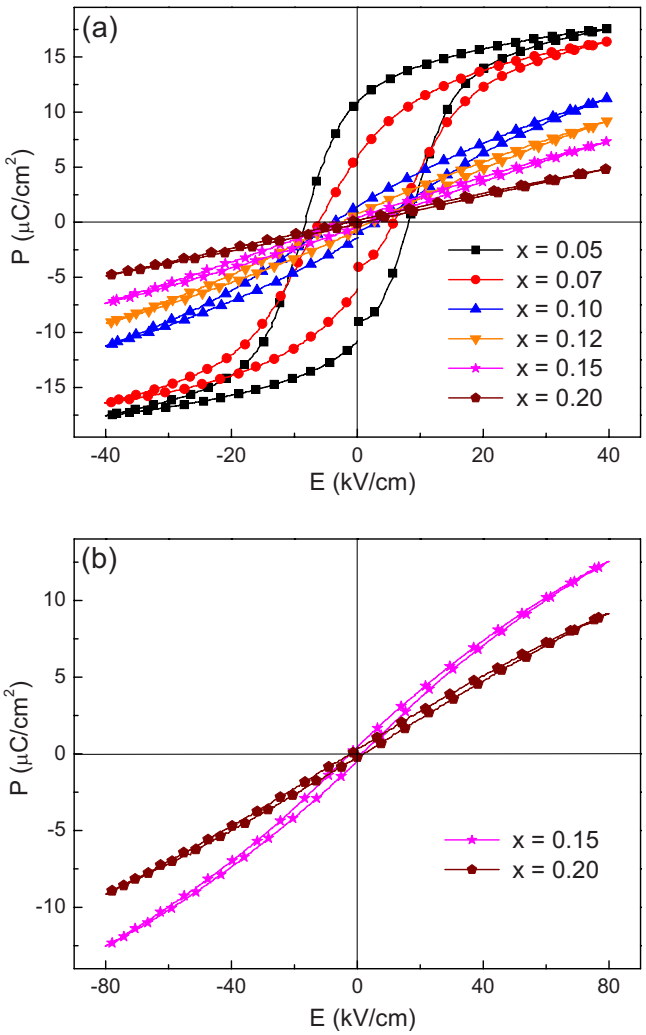

FIG. 5. (Color online) (a) Polarization P vs electric field E plots of $(1-x)BaTiO_3-xBi(Li_{1/3}Ti_{2/3})O_3$ ceramics measured at 4 Hz with 40 kV/cm peak field at room temperature. (b) P vs E plots for the composition $x=0.15$ and 0.20 measured at 4 Hz with 80 kV/cm peak field at room temperature.

P versus E curves become almost linear for samples with $x>0.12$ when tested with a peak field of 40 kV/cm. The trend of diminishing hysteresis with increasing amount of $Bi(Li_{1/3}Ti_{2/3})O_3$ in the present $(1-x)BaTiO_3-xBi(Li_{1/3}Ti_{2/3})O_3$ system is consistent with that in $(1-x)BaTiO_3-xBiScO_3$ and $(1-x)BaTiO_3-xBi(Zn_{1/2}Ti_{1/2})O_3$ (Refs. 13 and 15). However, when tested at a higher peak field of 80 kV/cm, the polarization starts to saturate [Fig. 5(b)], which is typical for a relaxor ferroelectric.

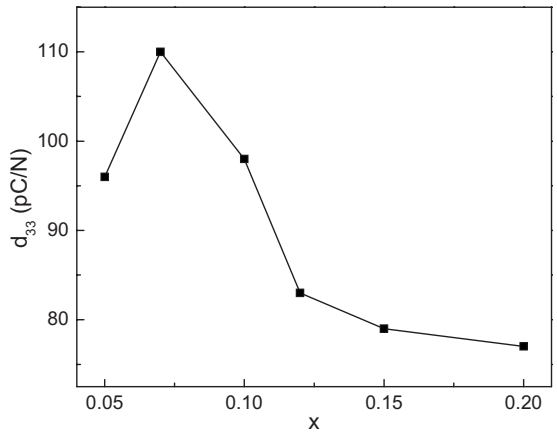

FIG. 6. The room temperature piezoelectric coefficient d_{33} as a function of composition x of $(1-x)BaTiO_3-xBi(Li_{1/3}Ti_{2/3})O_3$ ceramics.

TABLE I. The room temperature piezoelectric coefficient d_{33} in $(1-x)BaTiO_3-xBi(Li_{1/3}Ti_{2/3})O_3$ ceramics.

x	0.05	0.07	0.10	0.12	0.15	0.20
d_{33} (pC/N)	96	110	98	83	79	77

The room-temperature piezoelectric coefficient d_{33} as a function of composition was plotted in Fig. 6 and listed in Table I. A strong compositional dependence of d_{33} was observed. The sample with $x=0.07$, which is close to the MPB as demonstrated by the XRD patterns in Fig. 1, displays the best value of d_{33} as 110 pC/N. It is evident that the MPB between the orthorhombic and tetragonal perovskite phases plays an important role in enhancing the piezoelectric properties, as demonstrated previously in the composition of $Ba(Ti_{0.95}Zr_{0.05})O_3$. (Ref. 23) TEM observations indicate that the large ferroelectric domains of $BaTiO_3$ are disrupted by the addition of $Bi(Li_{1/3}Ti_{2/3})O_3$ around the MPB composition (Fig. 4). The instability in the domain structure might facilitate the polarization switching and thus improve the piezoelectricity.

IV. CONCLUSIONS

Lead-free perovskite ceramics of the $(1-x)BaTiO_3-xBi(Li_{1/3}Ti_{2/3})O_3$ $(0.05\leq x\leq 0.20)$ solid solution were synthesized via the conventional solid state reaction method. A MPB between tetragonal and orthorhombic perovskite phases was observed between the compositions $x=0.07$ and 0.10. The dielectric anomaly at ~130 °C in the ε_r versus T curves, associated with the ferroelectric-paraelectric phase transition, gets weaker while a relaxor behavior with a diffuse transition at a lower temperature gets stronger as the content of $Bi(Li_{1/3}Ti_{2/3})O_3$ increases. This trend is quantitatively demonstrated by the relaxation parameter and the diffuseness parameter. The observed dielectric behaviors are originated from the core-shell grain structure where large lamellar ferroelectric domains occupy the core and nanodomains are the features for the shell. The enhanced relaxor behavior diminishes both the remanent polarization and the coercive field. At the MPB composition $x=0.07$ with a mixed relaxor and normal ferroelectric behaviors, a piezoelectric coefficient d_{33} of 110 pC/N was observed.

ACKNOWLEDGMENTS

This set of results is based upon work supported by the Air Force Research Laboratory under Contract No. FA8650-04-C-5228 at Iowa State University's Center for NDE.

[1]B. Jaffe, W. R. Cook, and H. Jaffe, *Piezoelectric Ceramics* (Academic, London, 1971).
[2]L. E. Cross, Ferroelectrics **76**, 241 (1987).
[3]G. H. Haertling, J. Am. Ceram. Soc. **82**, 797 (1999).
[4]J. Rödel, W. Jo, K. Seifert, E. M. Anton, T. Granzow, and D. Damjanovic, J. Am. Ceram. Soc. **92**, 1153 (2009).

[5]R. Guo, L. E. Cross, S.-E. Park, B. Noheda, D. E. Cox, and G. Shirane, Phys. Rev. Lett. **84**, 5423 (2000).
[6]R. E. Cohen, Nature (London) **358**, 136 (1992).
[7]I. Grinberg, M. R. Suchomel, P. K. Davies, and A. M. Rappe, J. Appl. Phys. **98**, 094111 (2005).
[8]K. A. Schönau, L. A. Schmitt, M. Knapp, H. Fuess, R.-A. Eichel, H. Kungl, and M. J. Hoffmann, Phys. Rev. B **75**, 184117 (2007).
[9]N. A. Hill, J. Phys. Chem. B **104**, 6694 (2000).
[10]M. Fiebig, J. Phys. D: Appl. Phys. **38**, R123 (2005).
[11]R. Seshadri and N. A. Hill, Chem. Mater. **13**, 2892 (2001).
[12]R. E. Eitel, C. A. Randall, T. R. Shrout, P. W. Rehrig, W. Hackenberger, and S.-E. Park, Jpn. J. Appl. Phys., Part 1 **40**, 5999 (2001).
[13]H. Ogihara, C. A. Randall, and S. Trolier-McKinstry, J. Am. Ceram. Soc. **92**, 110 (2009).
[14]M. R. Suchomel and P. K. Davies, Appl. Phys. Lett. **86**, 262905 (2005).
[15]C. C. Huang and D. P. Cann, J. Appl. Phys. **104**, 024117 (2008).
[16]D. Fu, M. Endo, H. Taniguchi, T. Taniyama, and M. Itoh, Appl. Phys. Lett. **90**, 252907 (2007).
[17]D. I. Bilc and D. J. Singh, Phys. Rev. Lett. **96**, 147602 (2006).
[18]M. R. Suchomel, A. M. Fogg, M. Allix, H. Niu, J. B. Claridge, and M. J. Rosseinsky, Chem. Mater. **18**, 4987 (2006).
[19]K. Uchino and S. Nomura, Ferroelectr., Lett. Sect. **44**, 55 (1982).
[20]N. Vittayakorn, G. Rujijanagul, X. Tan, M. A. Marquardt, and D. P. Cann, J. Appl. Phys. **96**, 5103 (2004).
[21]D. Viehland, M.-C. Kim, Z. Xu, and J.-F. Li, Appl. Phys. Lett. **67**, 2471 (1995).
[22]C. A. Randall, D. J. Barber, R. W. Whatmore, and P. Groves, Ferroelectrics **76**, 311 (1987).
[23]Z. Yu, C. Ang, R. Guo, and A. S. Bhalla, J. Appl. Phys. **92**, 1489 (2002).